HHS Public Access

Author manuscript

Insect Biochem Mol Biol. Author manuscript; available in PMC 2022 April 15.

Published in final edited form as:

Insect Biochem Mol Biol. 2022 April ; 143: 103729. doi:10.1016/j.ibmb.2022.103729.

Sequence analysis and function of mosquito aeCCC2 and *Drosophila* Ncc83 orthologs

Phu C. Duong[a,1], **Tobias C. McCabe**[a,1], **Grace F. Riley**[a], **Heather L. Holmes**[b], **Peter M. Piermarini**[c], **Michael F. Romero**[b], **Christopher M. Gillen**[a,*]

[a]Department of Biology, Kenyon College, Gambier, OH, 43050, USA

[b]Physiology and Biomedical Engineering, Nephrology and Hypertension, Mayo Clinic College of Medicine and Science, Rochester, MN, 55902, USA

[c]Department of Entomology, The Ohio State University, Ohio Agricultural Research and Development Center, Wooster, OH, 44691, USA

Abstract

Dipteran insects have genes that code for two different Na^+-dependent cation-chloride cotransporter (CCC) paralogs. *Aedes aegypti* aeNKCC1 is an ortholog of *Drosophila melanogaster* Ncc69, a bumetanide-sensitive Na^+- K^+−$2Cl^-$ cotransporter (NKCC). *Aedes aegypti* aeCCC2 and aeCCC3 are orthologs of *Drosophila* Ncc83. Prior work suggests that the transport properties of aeCCC2 differ from canonical NKCCs. In particular, *Xenopus* oocytes expressing aeCCC2 have increased Na^+-dependent membrane currents compared to controls, whereas NKCCs are electroneutral. Here, we further evaluated the function and localization of aeCCC2 and Ncc83. In oocytes expressing aeCCC2 or Ncc83, membrane potential (V_m) hyperpolarized upon Na^+ removal; following hypotonic exposure the change in V_m was greater than it was in controls. In voltage-clamp experiments, membrane currents were concentration dependent on Na^+ with an apparent affinity (K_m) of approximately 4.6 mM. In Malpighian tubules of larval and adult mosquitoes, aeCCC2 was localized along the basolateral aspect of principal cells. Sequence comparisons among transporters from *Drosophila, Aedes, Anopheles*, and *Culex* revealed 33 residues within the transmembrane domains (TMDs) that are fully conserved within paralogs but that differ between orthologs of NKCC1 and orthologs of aeCCC2/Ncc83. These residues are distributed across all 12 TMDs. Our results provide a foundation for further exploration of the structural basis for functional differences between insect Na^+-dependent CCCs.

Keywords

Cation-chloride cotransporter; Membrane potential; Insects; Renal tubule; Epithelial transport

*Corresponding author: gillenc@kenyon.edu (C.M. Gillen).

[1]These authors contributed equally.

Appendix A. Supplementary data

Supplementary data to this article can be found online at https://doi.org/10.1016/j.ibmb.2022.103729.

1. Introduction

Despite their medical and physiological importance, solute transporters are understudied compared to other groups of proteins (César-Razquin et al., 2015). Moreover, because solute transporters are relatively well-conserved in structure yet diverse in function, predicting function from sequence comparisons can be difficult. For example, the cystic fibrosis transmembrane conductor regulator (CFTR) is a member of the ATP-binding-cassette (ABC) family of membrane proteins, which are mostly ATP-dependent pumps, but it functions instead as a Cl^- channel (Linsdell, 2018). Similarly, *Drosophila melanogaster* NHA1 is a member of the cation/proton antiporter (CPA, SLC9B) family but instead acts as a Cl^--proton cotransporter (Chintapalli et al., 2015). Additionally, the ClC-family includes both chloride channels and Cl^--proton exchangers (Jentsch and Pusch, 2018). Functional differences between closely related transporters arise because relatively small changes in primary amino acid sequence can result in dramatic changes in transport properties (Bacconi et al., 2005; Broër et al., 2009; Uzdavinys et al., 2017). Thus, functional characterization of solute transporters is especially necessary.

Members of the cation-chloride-cotransporter family (CCC, SLC12) have important roles in cell volume regulation, intracellular Cl^- regulation, and transepithelial salt movement (Arroyo et al., 2013; Haas, 1994; Russell, 2000). In mammals, CCCs include four K^+-Cl^- cotransporters (KCC, SLC12A4-SLC12A7), two Na^+-K^+−$2Cl^-$ cotransporters (NKCC, SLC12A1 and SLC12A2), one Na^+-Cl^- cotransporter (NCC, SLC12A3), CCC9 (SLC12A8), and CIP1 (SLC12A9) (Hartmann et al., 2014).

Recent cryo-electron microscopy (cryo-EM) structures confirm earlier work showing that the CCCs have 12 transmembrane domains (TMDs), with TMDs 1–10 forming an inverted repeat structure that is typical of the Amino Acid-Polyamine-Organocation (APC) superfamily of membrane transport proteins (Chew et al., 2019; Delpire and Guo, 2019; Liu et al., 2019; Yang et al., 2020; Zhang et al., 2021). TMDs 11 and 12 are mainly involved in dimerization. The cryo-EM structures also identify residues in TMDs 1, 3, 6, 8, and 10 as central to binding of Na^+, K^+, and Cl^- ions. For example, a tyrosine in TM3 of NKCC1 (Y383 in the human NKCC1 sequence) coordinates with potassium ions. The tyrosine is substituted with a histidine in NCC, consistent with the K^+-independence of NCC (Chew et al., 2019; Zhang et al., 2021).

Insects have genes coding for both KCCs and NKCCs (Hartmann et al., 2014; Pullikuth et al., 2003). *Drosophila melanogaster* Ncc69 (CG4357) is a canonical NKCC with 1:1:2 Na^+:K^+:Cl^- stoichiometry and high sensitivity to bumetanide (Leiserson et al., 2011; Sun et al., 2010). Additionally, insects have a clade of transporters (NaCCC2) that groups most closely to vertebrate NKCC and NCC but does not have direct mammalian orthologs (Piermarini et al., 2017). The NaCCC2 clade includes *Drosophila melanogaster* Ncc83 (CG31547), which is ~74% identical to Ncc69 across their transmembrane (TM) regions; this is about the same identity shared by human NCC and NKCC1. Mosquitoes have two NaCCC2s that probably resulted from a gene duplication early in mosquito evolution. In *Aedes aegypti*, the NaCCC2 paralogs are differentially expressed among tissues. AeCCC2

is abundant in hindgut of adults, whereas aeCCC3 is abundant in the anal papillae of larvae (Durant et al., 2021; Piermarini et al., 2017).

Flux assays and sequence comparisons suggest that insect NaCCC2s differ in function from NKCC1s. When aeCCC2 was expressed in *Xenopus* oocytes, uptake of the Na^+ tracer Li^+ increased, but uptake of the K^+ tracer Rb^+ was unchanged (Kalsi et al., 2019). Surprisingly, this Li^+ uptake was not dependent on extracellular Cl^- and was not affected by established Na^+-transporter inhibitors including furosemide, bumetanide, hydrochlorothiazide, and amiloride. In voltage clamp experiments, oocytes expressing aeCCC2 had a Na^+-dependent membrane current, suggesting that aeCCC2 conducts electrogenic movement of Na^+. The TM3 residue corresponding to hNKCC1 Y383 is substituted with an asparagine in aeCCC2 and aeCCC3, suggesting a structural basis for K^+-independence in these transporters (Piermarini et al., 2017).

Because they have strong structural similarity but apparently have quite different functional properties, comparisons of Ncc83 and aeCCC2 to NKCC1s may illuminate key structure-function properties of the CCCs. Here, we further explore the function and localization of dipteran NaCCC2s and evaluate sequence differences between NaCCC2 and NKCC1 orthologs from mosquitoes and *Drosophila*.

2. Methods

2.1 Exogenous expression in Xenopus laevis oocytes

As described previously, the aeCCC2 cDNA (AAEL009888) was synthesized and cloned into the oocyte expression plasma pGH19 by a commercial service (Kalsi et al., 2019). Plasmids containing ORFs for Ncc83 (GH09711) and Ncc69 (GH27027) were obtained from the Drosophila Genome Resource Center (Bloomington, IN), and the ORFs were subcloned into the pGEMHE oocyte expression vector. The full ORF of each construct was sequenced. cRNAs were transcribed from linearized plasmids using the T7 mMessage mMachine kit (Ambion). Following previously described procedures (Romero et al., 1998), isolated *X. laevis* oocytes were injected with 50 nl of cRNA in water (0.4–0.5 μg/μL, i.e., 20–25 ng per oocyte) or water. Oocytes were maintained in OR3 media at 16 °C and studied 3–7 days after injection.

2.2 Membrane potential (V_m)

For measurements of V_m, oocytes were placed in a chamber, perfused with ND96 solution, and impaled with a KCl microelectrode. Composition of ND96 was: 96 mM NaCl, 2.0 mM KCl, 1.8 mM $CaCl_2$, 1.0 mM $MgCl_2$, 5.0 mM HEPES, pH 7.5. V_m was measured as the difference between the potential of the KCl microelectrode and an extracellular calomel electrode. Na^+-dependent changes in V_m were assessed by switching between a Na^+-free solution (isotonic replacement of Na^+ with N-methyl-D-glucamine) and standard ND96, while maintaining constant chamber perfusion of approximately 5 ml/min.

To evaluate the activation of expressed cotransporters by swelling, we measured Na^+-dependent changes in V_m prior to and following a 10 min exposure to 50% hypotonic solutions. These exposures were either in standard ND96 or nominal Cl^- (0Cl-) ND96

(isotonic replacement of Cl^- with gluconate) diluted 1:1 with deionized water. No differences were observed between Na^+-dependent V_m responses following exposures to standard or 0 Cl^- hypotonic media, so those data were pooled for analysis.

Resting V_m, change in V_m upon Na^+ removal, change in V_m during hypotonic exposure, and rate of V_m recovery following Na^+ re-addition were calculated using the same standardized time intervals for each experiment. Resting V_m was mean V_m during the 60 s before the first Na^+ removal maneuver. The change in V_m was the difference between V_m during the last 10 s before Na^+ removal and the V_m during the last 10 s in Na^+ -free solution. Change in V_m during hypotonic exposure was the difference in V_m during the 10 s prior to hypotonic exposure and the final 10 s of hypotonic exposure. The rate of V_m recovery was the slope of V_m versus time over the first −60 s following Na^+ return with constant chamber perfusion.

Two-electrode voltage clamp: Oocytes were impaled with two KCl electrodes and perfused with Na^+-free ND96 (isotonic replacement of Na^+ with choline). After V_m stabilized, V_m was clamped at 60 mV. Na^+-dependent currents were measured by switching to solutions with Na^+ at concentrations ranging from 2 mM to 96 mM. In some experiments, Na^+ replacement was performed before and after exposure to hypotonic swelling as described above.

2.3. Immunohistochemistry

Aedes aegypti eggs (BEI Resources) were hatched in tap water under vacuum. Larvae were fed finely ground Total Goldfish® flakes and maintained at 28 °C, 80% humidity, and 14:10h light/dark cycle. Adults were fed 10% sucrose *ad libitum*. Fourth-instar larvae and adult mosquitoes were cold-anesthetized and dissected in Ringer solution. Whole guts were removed and fixed in 4% paraformaldehyde, rinsed 3 times in phosphate buffered sodium (PBS) and once in PBS-0.1% Triton X-100 (Sigma Aldrich), and blocked with 10% normal goat serum (NGS) and 1% casein in PBS-0.1% Tween for 1.5 h at RT.

Rabbit polyclonal antibodies were developed by a commercial supplier (ProteinTech, Chicago, IL) against aeCCC2 (C2–1-2) and aeCCC3 (C3–1-2) using peptides identified previously to be antigenic and unique to aeCCC2 (Cys-VDMHSKLLQHFTDNDGTQIP) and aeCCC3 (Cys-ISVNVPNEAQDNKTTPEA) (Piermarini et al., 2017). The C2–1 antibody brightly stained the plasma membrane of oocytes expressing aeCCC2 (supplemental Figure 1). No specific membrane staining by C2–1 was observed in oocytes expressing aeCCC3. Conversely, the C3–1 antibody stains plasma membranes of oocytes expressing aeCCC3 but not aeCCC2. To selectively stain stellate cells, we used the a5 monoclonal antibody against the Na^+-K^+-ATPase alpha-subunit, which was deposited to the Developmental Studies Hybridoma Bank (DSHB Hybridoma Product a5) by Fambrough, D.M. (Lebovitz et al., 1989).

Whole guts were incubated at 4 °C overnight with C2–1-2 primary antibody diluted 1:50 in PBS-0.1% Tween/Casein. Negative controls were incubated without primary antibody. Following three washes in PBS, samples were incubated with goat anti-rabbit Dylight-488 Fluor 2° antibody (1:200 in PBS/casein; Thermo Fisher) overnight at 4 °C or 1.5 h at RT. Tissues were treated with DAPI (Invitrogen; 5 min) to counterstain nuclei and then

washed once with PBS-0.1% Tween. Whole mounts were visualized with Nikon DS-L2 or with TCS SPS II confocal microscope with Leica Microsystems LAS AF software (Leica Microsystems).

Image analysis was performed within FIJI (ImageJ 1.52p).

2.4 Sequence analysis

Protein sequences from mosquito (*Aedes, Anopheles,* and *Culex*) and fruit fly (*Drosophila*) species were collected from Vectorbase and NCBI databases using protein BLAST searches with insect NKCC1s or NaCCC2 as queries. Sequence analysis was conducted using a set of customized R Markdown scripts (R 4.0.3). Sequences were aligned using ClustalO-mega at default parameters through the msa 1.22.0 package. Partial and duplicate sequences were identified and removed. Sequences from a species were not used in further analyses unless sequences for all paralogs (two for *Drosophila*; three for mosquitoes) were identified. For routine quality control, neighbor-joining phylogenetic trees were generated through pairwise distance alignment values using the seqinr 4.2–4 and ape 5.5 packages and rooted with vertebrate NKCC1 sequences. Phylogenetic relationships were also evaluated and visualized using Maximum Likelihood tree with default parameters and bootstrapping in MegaX 10.2.4. In total, we used sequences from 10 mosquito (2 *Aedes*, 1 *Culex*, and 7 *Anopheles*) and 10 *Drosophila* species (Supplemental Table 1). In some analyses, sequences from *H. sapiens* and *D. rerio* were used as reference sequences but were not included in conservation and consensus calculations. TMDs were defined according to human NKCC1 (hNKCC1) cryo-EM structures (Yang et al., 2020; Zhang et al., 2021). Throughout the paper, residues are numbered in reference to the numbering scheme of hNKCC1.

Amino acid sequence conservation was determined as percent identity compared to paralog-specific consensus sequences. For analysis of TMD domains, percent identity was calculated individually for each TMD of each sequence as the number of residues that match the consensus divided by total residues in the TMD and multiplied by 100. We also identified individual residues that were 100% conserved within each paralog but different between paralogs. These analyses were performed separately for mosquito and *Drosophila* sequences and for mosquito and *Drosophila* sequences combined. We compared these results to residues known to be involved in ion and inhibitor affinities or crucial for overall protein structure-function in vertebrate NKCC1 (Araújo et al., 2021; Chew et al., 2019; Somasekharan et al., 2012; Yang et al., 2020; Zhang et al., 2021).

2.5. Modeling

Figures were generated in Pymol using the published cryo-EM structure of hNKCC1 as reference (PDB: 6PZT) (Yang et al., 2020). After non-TMD residues and TMDs 11–12 were removed for visual clarity, annotated residues were highlighted in “ball-and-stick” model and colored based on TMD. Ions absent from the original PDB were retrieved from other published PDB structures and manually docked into reported binding sites (Chew et al., 2019; Yang et al., 2020).

2.6. Statistics

Data were assessed for normality by the Shapiro test and by inspection of histograms. When the assumption of normality was not justified, the non-parametric Kruskal-Wallis test was used to evaluate statistical significance of differences. Otherwise, ANOVAs with Tukey's post-hoc comparisons and paired t-tests were used. Central tendencies are reported as mean ± Box and whiskers plots (Figs. 2, 3 and 7) depict the interquartile range (IQR) with boxes, the range with whiskers, and the outliers (more than 1.5 times the IQR above or below the IQR) with dots.

3. Results

3.1. Oocyte experiments

We studied oocytes expressing aeCCC2, Ncc83, and Ncc69 in isotonic and hypotonic solutions because hypotonic swelling activates Na^+- dependent CCCs in vertebrates and insects (Dowd and Forbush, 2003; Murillo-de-Ozores et al., 2020; Rodan, 2018; Wu et al., 2014). Oocytes expressing aeCCC2 had different membrane potential (V_m) and responses to hypotonic swelling than oocytes injected with water or other expression constructs (Fig. 1). The aeCCC2 oocytes had a resting V_m of approximately −12 mV, approximately 20–30 mV more positive than oocytes injected with water, Ncc83, and Ncc69 (Fig. 2a, Kruskal-Wallis, $p < 0.01$). During hypotonic swelling, V_m of aeCCC2 oocytes increased, becoming more positive by 13.7 ± 6.5 mV (mean ± sd). In contrast, V_m of control and Ncc69 oocytes hyperpolarized, becoming more negative by 12–14 mV (Fig. 2b, ANOVA, Tukey's post-hoc test, $p < 0.001$). The V_m of Ncc83 oocytes hyperpolarized by only 3.1 ± 8.5 mV.

Prior to hypotonic swelling, removal of Na^+ produced only small changes in V_m in all treatments (Fig. 3a). In contrast, following 10 min exposure to hypotonic medium, oocytes expressing both aeCCC2 and Ncc83 had decreases in V_m of 26.5 ± 11.6 and 20.0 ± 6.2 mV, compared to mean declines in Ncc69 and water injected oocytes of less than 5 mV (Fig. 3b, ANOVA, Tukey's post-hoc test, $p < 0.05$). Following re-addition of Na^+, the rate of V_m recovery was faster in oocytes expressing aeCCC2 and Ncc83. Prior to swelling, mean rate of V_m increase was 0.80 ± 0.68 mV/s in aeCCC2 and 1.1 ± 1.2 mV/s in Ncc83 oocytes, compared to 0.16 ± 0.09 mV/s in water-injected and 0.11 ± 0.05 in Ncc69 oocytes (ANOVA, $p = 0.07$). Following swelling, recovery rate of V_m increased in aeCCC2 oocytes to 2.4 ± 1.3 mV/s and 1.7 ± 0.9 mV/s in Ncc83 oocytes, whereas that of water and Ncc69-injected oocytes remained lower than 0.15 mV/s. The recovery rates following hypotonic treatment in Ncc83 and aeCCC2 oocytes were significantly greater than those in Ncc69 oocytes and controls (ANOVA, $p < 0.001$).

In a separate series of experiments, we measured Na^+-dependent currents before and after a 10 min hypotonic exposure in voltage-clamped oocytes expressing aeCCC2. Prior to hypotonic treatment, current increased by 109 ± 56 mA ($n = 5$) upon returning Na^+ to oocytes held in 0 mM Na^+. Following hypotonic treatment, Na^+-dependent current was 165 ± 70 mA, and was greater in every oocyte compared to the pre-hypotonic condition in the same oocyte (paired *t*-test, p 0.04).

We evaluated the concentration dependence of membrane current on extracellular [Na^+] in oocytes expressing aeCCC2 at 60 mV. Following 10 min hypotonic exposure, we measured changes in current when oocytes were switched from 0 mM Na^+ to solutions with [Na^+] ranging from 2.4 to 96 mM (Fig. 4). Inward currents were observed in oocytes expressing aeCCC2 in response to returning Na^+. The magnitude of changes in current in response to Na^+ replacement was maximal (~200–300 nA) at [Na^+] of 24, 48, and 96 mM, only slightly smaller at 9.6 mM, and declined to ~50% of maximum at 4.8 mM (Fig. 4). The response to [Na^+] was consistent with simple Michaelis-Menten kinetics with an apparent affinity of 4.6 ± 1.1 mM (Fig. 4b, n = 5).

3.2. Immunohistochemistry

A polyclonal antibody against aeCCC2 (C2–1) stained the entire length of Malpighian tubules from adult and larval mosquitoes (Fig. 5). Staining of midgut and hindgut was also observed, but we did not further evaluate those tissues in this study. In larval tubules, staining was most prominent along the basolateral aspect of principal cells (Fig. 5A). Staining by C2–1 was largely absent from stellate cells (Fig. 5B and C). Staining along the basal margin was observed in both proximal (Fig. 5D) and distal portions of tubules (Fig. 5E) when Z-sections across the tubule were averaged and also in single 1 μM Z-sections (Supplementary Fig. 2A and B). Some variation between tubules in the pattern of staining by C2–1 was noted, with staining in certain tubules less distinctly restricted to the basal margin (Fig. 5F and supplemental Figure 2C). However, staining of the apical membrane by C2–1 was never observed. In Malpighian tubules of adult female mosquitoes, staining by C2–1 also primarily occurred along the basolateral aspect of principal cells, but punctate intracellular labelling was also observed (Fig. 5G). As expected, the A5 antibody against the Na^+−K^+-ATPase stains stellate cells of larval Malpighian tubules (supplemental Figure 2C) (Patrick et al., 2006). No staining was observed in negative controls in which primary antibody was omitted (Supplementary Figure 2D).

3.3. Sequence analysis

The amino acid sequences used in this analysis grouped as expected (Fig. 6). To evaluate differences in conservation among paralogs, we separately calculated percent amino acid identity of mosquito and fruit fly sequences to their paralog-specific consensus sequences. Absolute conservation values may differ between the mosquito and *Drosophila* sequences simply because of the evolutionary distances between the selected species, especially because we collected sequences from three genera of mosquitos. For this reason, we focus on differences in the patterns of conservation among paralogs and TMDs within mosquito and *Drosophila* instead of differences in absolute conservation between the groups.

Across all twelve TMDs in mosquitos, NKCC1 has the highest percent identity (95.3%), followed by CCC3 (92.2%) and CCC2 (89.9%) (Kruskal-Wallis, p 0.003). In contrast, CCC2 (97.2%) is better conserved than NKCC1 (94.3%) in fruit flies (Kruskal-Wallis, $p < 0.001$). Thus, NKCC1 is better conserved in mosquitoes whereas CCC2 is better conserved in fruit flies.

To evaluate differences among TMDs, we compared percent conservation of amino acids among TMDs of mosquitoes and fruit flies. TMDs differed in their percent identity (Kruskal-Wallis, $p < 0.001$). The most highly conserved TMDs are 1, 6, 8, and 10. In fruit flies, percent identity is 99.7% or greater across those TMDs in CCC2 and 97.1% or greater in NKCC1 (Fig. 7b). The same pattern is found in mosquitoes (Fig. 7a). Percent identity is greater than 94.5% in TMDs 1, 6, 8 and 10 for NKCC1, CCC2, and CCC3, except for TMD 10 in CCC3 (91.3%). *Aedes* and *Culex* sequences differ to a greater extent than *Anopheles* sequences from the consensus sequence, probably because the majority of sequences in the analysis were from *Anopheles*.

Conservation of TMD2 and TMD3 differs between both species and paralogs. In fruit flies, TMD2 is more highly conserved in NKCC1 (97.8%) than CCC2 (91.9%), but TMD3 is less highly conserved in NKCC1 (91.9%) compared to CCC2 (97.8%). In mosquitoes, TMD2 is only moderately conserved in all three paralogs (89.6%–91.9%). However, TMD3 is highly conserved in NKCC1 and CCC3 (97.5% and 96.4%), but less well conserved in CCC2. In summary, TMD2 is best conserved in fruit fly NKCC1, whereas TMD3 is best conserved in fruit fly CCC2 and mosquito NKCC1 and CCC3.

3.4. Single residue analysis

To explore which amino acid residues might contribute to the functional differences between NaCCC2s and NKCC1, we identified residues that are 100% conserved within both CCC2 and NKCC1 but differ between the paralogs (Fig. 7, Table 1). Of 307 residues in the 12 TMDs, 33 meet this criterion, including at least one residue from every TMD. TMD3 has 7 such residues, TMD8 and TMD10 have 5 each, and TMD2 has 4. Of the 33 residues, at least 12 were previously identified as functionally or structurally important residues in NKCC1 or CCC2 (Araújo et al., 2021; Chew et al., 2019; Dehaye et al., 2003; Gagnon et al., 2002; Isenring et al., 1998; Payne, 2012; Somasekharan et al., 2012; Yang et al., 2020; Zhang et al., 2021). For a third of the identified residues, the amino acid substitutions are relatively conservative swaps between small hydrophobic amino acids (A, I, L, and V). Only one instance involves a charged residue – the substitution of R in NKCC1 with P in CCC2 (R294 in hNKCC1 numbering) in TMD1. In 7 cases, the substitutions involve changes in polarity. Notable examples include the substitution of Y383 in NKCC1 with N in CCC2 in TMD3 and the substitution of A497 in NKCC1 with S in CCC2 in TMD6. Residue 502 in TMD6 is worth noting even though it does not meet the criteria of 100% identical in NKCC1 and NaCCCs. This residue is a L in NKCC1 and a Q in all *Drosophila* CCC2, all mosquito CCC3s, and 90% of mosquito CCC2s. In *Anopheles merus,* this residue is a H rather than a Q. When mapped onto hNKCC1, the conserved differences cluster towards the core of the transporters and tend to orient towards the ion binding sites (Fig. 8).

In the intracellular loops (ICL) and extracellular loops (ECL) between TMDs, 7 residues meet the criteria of 100% conserved within but different between NKCC1 and NaCCC2s of mosquitoes and *Drosophila* (Supplemental Table 2). Of particular interest are one site in EL3 where in NaCCC2s S substitutes for N469 and two sites in EL4 where in NaCCC2s Q substitutes for E594 and M substitutes for V596.

SPAK kinases activate Na^+-dependent CCCs (Dowd and Forbush, 2003; Murillo-de-Ozores et al., 2020; Rodan, 2018; Wu et al., 2014). We assessed whether the mosquito and *Drosophila* sequence have consensus Ste20-related proline alanine-rich kinase (SPAK) binding and phosphoacceptor sites (Delpire and Gagnon, 2007; Gagnon and Delpire, 2010). The consensus SPAK binding site (RFx[V/I]xx[V/I/T/S] is present in all *Drosophila* and mosquito NKCC1s, *Drosophila* CCC2s, and *Aedes* CCC2 and CCC3 (Supplemental Figure 3). However, it is absent in *Anopheles* CCC3 sequences, and in *Anopheles* CCC2 sequences, RF is substituted with QY. Four nearby threonine residues are SPAK phosphoacceptor sites in vertebrates (Gagnon and Delpire, 2010). These sites are variously conserved in the dipteran sequences (Supplemental Figure 4). Notably, a S replaces T at the third site in all the sequences except *Anopheles* CCC2. This S is followed in every case by a hydrophobic residue, a functional requirement in vertebrate NKCC1 (Gagnon and Delpire, 2010). The fourth site is conserved as a T in all sequences except *Anopheles* CCC3s.

4. Discussion

Our physiological findings support the hypothesis that the NaCCC2s, including aeCCC2 and Ncc83, are electrogenic sodium transporters. We also found conserved differences between insect NaCCC2s and NKCC1s across the TMDs, suggesting that widespread changes in primary sequence underpin the functional differences between NaCCC2s and NKCC1s.

4.1 Electrophysiology

In previous work, oocytes expressing aeCCC2 had increased Li^+ up-take and Na^+-dependent current compared to water injected controls (Kalsi et al., 2019). The Li^+ uptake was not dependent upon external Cl^- or inhibited by bumetanide, suggesting functional differences from Na^+-K^+-Cl^- cotransporters. Here, we show that following hypotonic swelling, oocytes expressing both Ncc83 and aeCCC2 have greater hyperpolarization in response to Na^+ removal than controls. Thus, these effects on transport physiology are not unique to oocytes expressing aeCCC2, but more generally reflect response to expression of NaCCC2s. As explained below, our results strongly suggest that aeCCC2 and Ncc83 are directly responsible for the Na^+-dependent electrogenic behavior. Although we cannot fully rule out the possibility that activation of an endogenous conductance in the oocytes also contributes to some of the electrical activity we detect, the Na^+ conductances we describe here differ from the endogenous voltage-gated and ligand-gated sodium channels described in oocytes (Antoine et al., 2007; Terhag et al., 2010).

Oocytes expressing Ncc83 and aeCCC2 had different resting V_m and responses to hypotonic swelling. Consistent with prior work (Kalsi et al., 2019), oocytes expressing aeCCC2 had depolarized resting V_m compared to control oocytes (Fig. 2a). However, V_m of oocytes expressing Ncc83 did not differ from controls. Depolarization of resting V_m in oocytes expressing aeCCC2 might be because aeCCC2 is partly activated in isotonic conditions. The unchanged resting V_m in oocytes expressing Ncc83 argues against the possibility that responses of oocytes to Na^+ removal are an indirect result of changes in resting V_m, since oocytes expressing Ncc83 have the response to Na^+ removal but do not have altered resting V_m. Oocytes expressing aeCCC2 differed from all other treatments in their increase in

V_m during hypotonic swelling. This depolarization could be due to activation of a Na^+ conductance mediated by aeCCC2 during hypotonic treatment.

Differences in the V_m response to Na^+ removal between controls and oocytes expressing aeCCC2 and Ncc83 were only observed after hypotonic swelling (Fig. 3). This result suggests that aeCCC2 and Ncc83 are activated by swelling, and is consistent with prior work in which oocytes expressing aeCCC2 were studied after hypotonic swelling (Kalsi et al., 2019). However, although swelling is the most likely explanation for the activation of Na^+ conductance, it is also possible that other factors – such as the change in membrane potential during the first Na^+ removal or Na^+ removal and replacement itself – might be involved. The similar activation of Na^+ conductances by hypotonic treatment of voltage-clamped oocytes expressing aeCCC2 argue against these other factors, since there was no change in V_m during these experiments and they were exposed to Na^+-free solution prior to the pre-swelling assessment of Na^+-dependent current. Activation of aeCCC2 and Ncc83 by swelling is expected because they contain binding and phosphorylation sites for SPAK (Supplemental Figures 3 and 4); and SPAK is known to upregulate CCCs in response to hypotonic swelling in vertebrates and insects (Dowd and Forbush, 2003; Murillo-de-Ozores et al., 2020; Rodan, 2018; Wu et al., 2014).

The response of oocytes expressing aeCCC2 to removal and return of Na^+ in voltage clamp experiments (Fig. 4) was consistent with previous work (Kalsi et al., 2019). Furthermore, saturation of the current response to Na^+ return at relatively low Na^+ concentrations suggests a carrier mechanism rather than a channel. In this experiment, the apparent Na^+ affinity of aeCCC2 is 4.6 mM. This K_m is approximately the same as the value determined for Ncc69 (7.4 mM) in one study (Leiserson et al., 2011) and considerably lower than the value (~50 mM) measured in another study (Sun et al., 2010).

4.2. Sequence analysis

Cryo-EM studies show that TMDs 1, 3, 6, 8, and 10 are particularly important in forming ion-binding sites of vertebrate NKCC1 (Chew et al., 2019; Yang et al., 2020; Zhang et al., 2021). These TMDs are also mostly well-conserved in insect NaCCC2s, suggesting that they also have key functional roles in the NaCCC2s (Fig. 7). A partial exception is TMD3, which is highly conserved in *Drosophila* CCC2s but less so in mosquito CCC2s. This difference follows the general trend of greater conservation of *Drosophila* CCC2s compared to mosquito CCC2s and CCC3s. The gene duplication that resulted in the CCC2 and CCC3 paralogs in mosquitoes may have reduced constraint and made possible diversification of these paralogs into new functional roles, resulting in the observed variation. Such variation in TMD3 might be especially central in shaping functional properties, given the known functional importance of TMD3 (Somasekharan et al., 2012).

The results of our comparison of the mosquito and *Drosophila* NaCCC2s to NKCC1s support the conclusion that the NaCCC2s differ substantially in function from NKCC1s. Most notably, dipteran NaCCC2s have a conserved substitution of R for Y at residue 383 in TMD3, consistent with previous work (Piermarini et al., 2017). According to recent cryo-EM studies, this residue coordinates K+ ions (Chew et al., 2019) and in vertebrate K^+-independent NCCs this residue is H rather than Y. Thus, this conserved substitution may

at least partly explain the lack of K^+ transport by aeCCC2 (Kalsi et al., 2019). Similarly, R294 in TMD1 and L502 in TMD6 have been implicated in Cl^- binding of NKCC1 (Chew et al., 2019), so the substitutions of P at residue 294 and Q at residue 502 are consistent with insect NaCCC2s performing Cl^--independent, electrogenic transport (Kalsi et al., 2019).

The conserved substitution of S for A in residue 497 in TMD6 may also contribute to the functional differences between NKCC1 and NaCCC2s. Mutation of this residue to a cysteine results in a non-functional protein, and a recent modeling study suggests that this residue may contribute to sensitivity of CCC2 and CCC3 to cinnamic acid (Araújo et al., 2021; Dehaye et al., 2003). Another intriguing set of substitutions is at or near residues that coordinate with Na^+ in TMD8. In NKCC1, the side chain oxygen of S614 coordinates with Na^+ and KCCs have a G at this site (Chew et al., 2019). This residue is substituted with T in NaCCC2s, a conservative substitution that maintains the coordinating side-chain oxygen but might influence the geometry of the binding pocket. Moreover, in KCCs, Q replaces S at position 618, whereas NaCCC2s have an N at this position. Finally, conserved differences between NKCC1 and NaCCC2s in the EL3 and EL4 are intriguing because these extracellular loops interact with the extracellular end of TMD1 in hNKCC1 (Yang et al., 2020). The functional significance of these substitutions as well as the others reported in Table 1 and supplemental Table 2 are unknown, but they are attractive candidates for future site-directed mutagenesis experiments.

Conserved differences between the dipteran NKCC1s and NaCCC2s are found across all 12 TMDs. This finding suggests that the evolutionary transition between ancestral NKCC1s and NaCCC2s required widespread structural adjustments, including changes in TMDs that do not directly coordinate with ions. TMD2 is particularly intriguing, because although it does not directly bind ions, prior work has suggested that it influences key functional properties such as ion binding affinities (Gimenez and Forbush, 2007; Payne, 2012). Intriguingly, the conserved differences between dipteran NaCCC2s and NKCC1s in TMD2 orient inward towards TMD6 and the ion binding pockets, suggesting that they might exert an influence indirectly through their interactions with TMD6 and other TMDs (Fig. 8). Overall, the sequence analysis suggests a complicated set of substitutions resulted in the divergence of insect NaCCC2s from NKCC1.

4.3. Localization

The C2–1 antibody raised against aeCCC2 stained the basolateral margin of principal cells of Malpighian tubules. The basolateral location of aeCCC2 matches the proposed localization of NKCCs in both *Drosophila* and mosquitoes (Piermarini et al., 2011; Rodan, 2019). In contrast, in the midgut of tobacco hornworm (*Manduca sexta),* the aeCCC2 ortholog msBSC is expressed apically (Gillen et al., 2006). Tissue-dependent localization has been observed for mosquito ATPases (Patrick et al., 2006) and MdNKCC2, a NaCCC2 ortholog from housefly *Musca domestica* (Barroso et al., 2020). Some tubules lacked distinct staining by C2–1 on the basolateral margin, but instead showed intracellular staining. This variability could reflect regulatory differences. Na^+-dependent CCCs can be activated by translocation from intracellular vesicles into the plasma membrane (D'Andrea-Winslow et al., 2001).

4.4 Summary and implications

The functional data and sequence analysis presented here support the hypothesis that insect NaCCC2s, including aeCCC2 and Ncc83, are electrogenic Na^+ transporting proteins (Kalsi et al., 2019). Moreover, the localization of aeCCC2 is consistent with possibility that it could contribute to the basolateral Na^+ conductance of mosquito Malpighian tubules measured in prior studies by other groups (Beyenbach and Masia, 2002; Hegarty et al., 1991; Sawyer and Beyenbach, 1985). Na^+ secretion is rapidly activated in tubules following a blood meal in female mosquitoes via the activation of a Na^+ conductance that depolarizes the basolateral membrane (Beyenbach and Petzel, 1987; Coast et al., 2005; Kwon et al., 2012; Williams et al., 1983). Our finding that oocytes expressing aeCCC2 exhibit an increased Na^+-dependent conductance and depolarization of V_m following hypotonic treatment prompts the hypothesis that aeCCC2 could contribute to this post-blood meal Na^+ conductance and natriuresis. In *Drosophila* tubules, the NKCC1 paralog Ncc69 was found to mainly contribute to K^+ secretion following stimulation (Rodan, 2019), with Na^+ probably recycling through the basolateral Na^+–K^+-ATPase of principal cells. If Ncc83 is a K^+-independent Na^+ transporter, then it could provide an additional pathway for Na^+ and thus contribute to tubular Na^+ secretion. Further characterization of NaCCC2s in expression systems as well as in intact tissues is needed to test these hypotheses.

Supplementary Material

Refer to Web version on PubMed Central for supplementary material.

Acknowledgements

Research reported in this publication was supported by National Institute of General Medical Science of the National Institutes of Health to CMG: R15-GM139088 and F33-GM131599. The content is solely the responsibility of the authors and does not necessarily represent the official views of the National Institutes of Health. CMG was also supported by an American Physiological Society Research Career Enhancement Award. We are grateful to Drs. Min-Hwang Chang, Matthew Rouhier, and Kathy Gillen for technical advice and assistance. We also thank Dr. Tea Meulia and MCIC staff. The following reagent was obtained through BEI Resources, NIAID, NIH: *Aedes aegypti*, Strain LVP-IB12, Eggs, MRA-735, contributed by David W. Severson. Plasmids containing ORFs of Drosophila Ncc69 and Ncc84 were obtained from the Drosophila Genomic Resource Center, Bloomington, IN.

References

Antoine A-F, Montpellier C, Cailliau K, Browaeys-Poly E, Vilain J-P, Dubuisson J, 2007. The alphavirus 6K protein activates endogenous ionic conductances when expressed in Xenopus oocytes. J. Membr. Biol 215, 37–48. 10.1007/s00232-007-9003-6. [PubMed: 17483865]

Araújo MO, Pérez-Castillo Y, Oliveira LHG, Nunes FC, Sousa D.P. de, 2021. Larvicidal activity of cinnamic acid derivatives: investigating alternative products for Aedes aegypti L. Control. Molecules 26. 10.3390/molecules26010061.

Arroyo JP, Kahle KT, Gamba G, 2013. The SLC12 family of electroneutral cation-coupled chloride cotransporters. Mol. Aspect. Med 34, 288–298. 10.1016/j.mam.2012.05.002.

Bacconi A, Virkki LV, Biber J, Murer H, Forster IC, 2005. Renouncing electroneutrality is not free of charge: switching on electrogenicity in a Na^+-coupled phosphate cotransporter. Proc. Natl. Acad. Sci. U.S.A 102, 12606–12611. 10.1073/pnas.0505882102. [PubMed: 16113079]

Barroso IG, Fuzita FJ, Ferreira C, Terra WR, 2020. Midgut fluxes and digestive enzyme recycling in Musca domestica: a molecular approach. Comp. Biochem. Physiol. A. Mol. Integr. Physiol 241, 110627. 10.1016/j.cbpa.2019.110627. [PubMed: 31812672]

Beyenbach K, Petzel D, 1987. Diuresis in mosquitoes: role of a natriuretic factor. Physiology 2, 171–175. 10.1152/physiologyonline.1987.2.5.171.

Beyenbach KW, Masia R, 2002. Membrane conductances of principal cells in Malpighian tubules of *Aedes aegypti*. J. Insect Physiol 48, 375–386. 10.1016/S0022-1910(02)00057-4. [PubMed: 12770112]

Bröer S, Schneider H-P, Bröer A, Deitmer JW, 2009. Mutation of asparagine 76 in the center of glutamine transporter SNAT3 modulates substrate-induced conductances and Na binding. J. Biol. Chem 284, 25823–25831. 10.1074/jbc.M109.031013. [PubMed: 19596860]

César-Razquin A, Snijder B, Frappier-Brinton T, Isserlin R, Gyimesi G, Bai X, Reithmeier RA, Hepworth D, Hediger MA, Edwards AM, Superti-Furga G, 2015. A call for systematic Research on solute carriers. Cell 162, 478–487. 10.1016/j.cell.2015.07.022. [PubMed: 26232220]

Chew TA, Orlando BJ, Zhang J, Latorraca NR, Wang A, Hollingsworth SA, Chen D-H, Dror RO, Liao M, Feng L, 2019. Structure and mechanism of the cation–chloride cotransporter NKCC1. Nature 572, 488–492. 10.1038/s41586-019-1438-2. [PubMed: 31367042]

Chintapalli VR, Kato A, Henderson L, Hirata T, Woods DJ, Overend G, Davies SA, Romero MF, Dow JAT, 2015. Transport proteins NHA1 and NHA2 are essential for survival, but have distinct transport modalities. Proc. Natl. Acad. Sci. Unit. States Am 112, 11720. 10.1073/pnas.1508031112.

Coast GM, Garside CS, Webster SG, Schegg KM, Schooley DA, 2005. Mosquito natriuretic peptide identified as a calcitonin-like diuretic hormone in *Anopheles gambiae* (Giles). J. Exp. Biol 208, 3281–3291. 10.1242/jeb.01760. [PubMed: 16109890]

D'Andrea-Winslow L, Strohmeier GR, Rossi B, Hofman P, 2001. Identification of a sea urchin Na(+)/K(+)/2Cl(−) cotransporter (NKCC): microfilament-dependent surface expression is mediated by hypotonic shock and cyclic AMP. J. Exp. Biol 204, 147–156. 10.1242/jeb.204.1.147. [PubMed: 11104718]

Dehaye JP, Nagy A, Premkumar A, Turner RJ, 2003. Identification of a functionally important conformation-sensitive region of the secretory Na^{+}-K^{+}−$2Cl^{-}$ cotransporter (NKCC1). J. Biol. Chem 278, 11811–11817. 10.1074/jbc.M213148200. [PubMed: 12556450]

Delpire E, Gagnon KBE, 2007. Genome-wide analysis of SPAK/OSR1 binding motifs. Physiol. Genom 28, 223–231. 10.1152/physiolgenomics.00173.2006.

Delpire E, Guo J, 2019. Cryo-EM structures of DrNKCC1 and hKCC1: a new milestone in the physiology of cation-chloride cotransporters. Am. J. Physiol. Cell Physiol 318, C225–C237. 10.1152/ajpcell.00465.2019. [PubMed: 31747317]

Dowd BFX, Forbush B, 2003. PASK (Proline-Alanine-rich STE20-related kinase), a regulatory kinase of the Na-K-Cl cotransporter (NKCC1). J. Biol. Chem 278, 27347–27353. 10.1074/jbc.M301899200. [PubMed: 12740379]

Durant AC, Grieco Guardian E, Kolosov D, Donini A, 2021. The transcriptome of anal papillae of Aedes aegypti reveals their importance in xenobiotic detoxification and adds significant knowledge on ion, water and ammonia transport mechanisms. J. Insect Physiol 132, 104269. 10.1016/j.jinsphys.2021.104269. [PubMed: 34174320]

Gagnon KB, Delpire E, 2010. On the substrate recognition and negative regulation of SPAK, a kinase modulating Na -K −2Cl cotransport activity. Am. J. Physiol. Cell Physiol 299, C614–C620. 10.1152/ajpcell.00074.2010. [PubMed: 20463172]

Gagnon É, Forbush B, Flemmer AW, Giménez I, Caron L, Isenring P, 2002. Functional and molecular characterization of the shark renal Na-K-Cl cotransporter: novel aspects. Am. J. Physiol. Ren. Physiol 283, F1046–F1055. 10.1152/ajprenal.00107.2002.

Gillen CM, Blair CR, Heilman NR, Somple M, Stulberg M, Thombre R, Watson N, Gillen KM, Itagaki H, 2006. The cation-chloride cotransporter, masBSC, is widely expressed in *Manduca sexta* tissues. J. Insect Physiol 52, 661–668. [PubMed: 16730744]

Gimenez I, Forbush B, 2007. The residues determining differences in ion affinities among the alternative splice variants F, A, and B of the mammalian renal Na-K-Cl cotransporter (NKCC2). J. Biol. Chem 282, 6540–6547. 10.1074/jbc.M610780200. [PubMed: 17186942]

Haas M, 1994. The Na-K-Cl cotransporters. Am. J. Physiol. Cell Physiol 36 267, C869–C885.

Hartmann A-M, Tesch D, Nothwang HG, Bininda-Emonds ORP, 2014. Evolution of the cation chloride cotransporter family: ancient origins, gene losses, and subfunctionalization through duplication. Mol. Biol. Evol 31, 434–447. 10.1093/molbev/mst225. [PubMed: 24273324]

Hegarty JL, Zhang B, Pannabecker TL, Petzel DH, Baustian MD, Beyenbach KW, 1991. Dibutyryl cAMP activates bumetanide-sensitive electrolyte transport in Malpighian tubules. Am. J. Physiol. Cell Physiol 261, C521–C529.

Isenring P, Jacoby SC, Forbush B, 1998. The role of transmembrane domain 2 in cation transport by the Na–K–Cl cotransporter. Proc. Natl. Acad. Sci. Unit. States Am 95, 7179–7184.

Jentsch TJ, Pusch M, 2018. CLC chloride channels and transporters: structure, function, physiology, and disease. Physiol. Rev 98, 1493–1590. 10.1152/physrev.00047.2017. [PubMed: 29845874]

Kalsi M, Gillen C, Piermarini PM, 2019. Heterologous expression of Aedes aegypti cation chloride cotransporter 2 (aeCCC2) in Xenopus laevis oocytes induces an enigmatic Na^+/Li^+ conductance. Insects 10, 71. 10.3390/insects10030071.

Kumar S, Stecher G, Li M, Knyaz C, Tamura K, 2018. Mega X: molecular evolutionary genetics analysis across computing platforms. Mol. Biol. Evol 35, 1547–1549. 10.1093/molbev/msy096. [PubMed: 29722887]

Kwon H, Lu H-L, Longnecker MT, Pietrantonio PV, 2012. Role in diuresis of a calcitonin receptor (GPRCAL1) expressed in a distal-proximal gradient in renal organs of the mosquito Aedes aegypti (L.). PLoS One 7, e50374. 10.1371/journal.pone.0050374. [PubMed: 23209727]

Lebovitz RM, Takeyasu K, Fambrough DM, 1989. Molecular characterization and expression of the (NaK)-ATPase alpha-subunit in Drosophila melanogaster. EMBO J 8, 193–202. 10.1002/j.1460-2075.1989.tb03364.x. [PubMed: 2540956]

Leiserson WM, Forbush B, Keshishian H, 2011. Drosophila glia use a conserved cotransporter mechanism to regulate extracellular volume. Glia 59, 320–332. [PubMed: 21125654]

Linsdell P, 2018. Cystic fibrosis transmembrane conductance regulator (CFTR): making an ion channel out of an active transporter structure. Channels 12, 284–290. 10.1080/19336950.2018.1502585. [PubMed: 30152709]

Liu S, Chang S, Han B, Xu L, Zhang M, Zhao C, Yang W, Wang F, Li J, Delpire E, Ye S, Bai X, Guo J, 2019. Cryo-EM structures of the human cation-chloride cotransporter KCC1. Science 366, 505. 10.1126/science.aay3129. [PubMed: 31649201]

Murillo-de-Ozores AR, Chávez-Canales M, de los Heros P, Gamba G, Castañeda-Bueno M, 2020. Physiological processes modulated by the chloride-sensitive WNK-SPAK/OSR1 kinase signaling pathway and the cation-coupled chloride cotransporters. Front. Physiol 11, 1353. 10.3389/fphys.2020.585907.

Patrick ML, Aimanova K, Sanders HR, Gill SS, 2006. P-type Na /K-ATPase and V-type H -ATPase expression patterns in the osmoregulatory organs of larval and adult mosquito Aedes aegypti. J. Exp. Biol 209, 4638–4651. 10.1242/jeb.02551. [PubMed: 17114398]

Payne JA, 2012. Molecular operation of the cation chloride cotransporters: ion binding and inhibitor interaction. Curr. Top. Membr 70, 215–237. 10.1016/B978-0-12-394316-3.00006-5. [PubMed: 23177987]

Piermarini PM, Akuma DC, Crow JC, Jamil TL, Kerkhoff WG, Viel KCMF, Gillen CM, 2017. Differential expression of putative sodium-dependent cation-chloride cotransporters in *Aedes aegypti*. Comp. Biochem. Physiol. A. Mol. Integr. Physiol 214, 40–49. 10.1016/j.cbpa.2017.09.007. [PubMed: 28923771]

Piermarini PM, Hine RM, Schepel M, Miyauchi J, Beyenbach KW, 2011. Role of an apical K,Cl cotransporter in urine formation by renal tubules of the yellow fever mosquito (*Aedes aegypti*). Am. J. Physiol. Regul. Integr. Comp. Physiol 301, R1318–R1337. 10.1152/ajpregu.00223.2011. [PubMed: 21813871]

Pullikuth AK, Filippov V, Gill SS, 2003. Phylogeny and cloning of ion transporters in mosquitoes. J. Exp. Biol 206, 3857–3868. 10.1242/jeb.00641. [PubMed: 14506221]

Rodan AR, 2019. The *Drosophila* Malpighian tubule as a model for mammalian tubule function. Curr. Opin. Nephrol. Hypertens 28, 455–464. 10.1097/mnh.0000000000000521. [PubMed: 31268918]

Rodan AR, 2018. WNK-SPAK/OSR1 signaling: lessons learned from an insect renal epithelium. Am. J. Physiol. Ren. Physiol 315, F903–F907. 10.1152/ajprenal.00176.2018.

Romero MF, Fong P, Berger UV, Hediger MA, Boron WF, 1998. Cloning and functional expression of rNBC, an electrogenic Na - HCO 3 cotransporter from rat kidney. Am. J. Physiol. Ren. Physiol 274, F425–F432. 10.1152/ajprenal.1998.274.2.F425.

Russell JM, 2000. Sodium-potassium-chloride cotransport. Physiol. Rev 80, 211–276. [PubMed: 10617769]

Sawyer DB, Beyenbach KW, 1985. Dibutyryl-cAMP increases basolateral sodium conductance of mosquito Malpighian tubules. Am. J. Physiol 248, R339–R345. [PubMed: 2579589]

Somasekharan S, Tanis J, Forbush B, 2012. Loop diuretic and ion-binding residues revealed by scanning mutagenesis of transmembrane helix 3 (TM3) of Na-K-Cl cotransporter (NKCC1). J. Biol. Chem 287, 17308–17317. 10.1074/jbc.M112.356014. [PubMed: 22437837]

Sun Q, Tian E, Turner RJ, Ten Hagen KG, 2010. Developmental and functional studies of the SLC12 gene family members from *Drosophila melanogaster*. Am. J. Physiol. Cell Physiol 298, C26–C37. 10.1152/ajpcell.00376.2009. [PubMed: 19828839]

Terhag J, Cavara NA, Hollmann M, 2010. Cave Canalem: how endogenous ion channels may interfere with heterologous expression in Xenopus oocytes. Xenopus Oocytes Exp. Syst 51, 66–74. 10.1016/j.ymeth.2010.01.034.

Uzdavinys P, Coinçon M, Nji E, Ndi M, Winkelmann I, von Ballmoos C, Drew D, 2017. Dissecting the proton transport pathway in electrogenic Na /H antiporters. Proc. Natl. Acad. Sci. Unit. States Am 114 10.1073/pnas.1614521114. E1101–E1110.

Williams JC, Hagedorn HH, Beyenbach KW, 1983. Dynamic changes in flow rate and composition of urine during the post-bloodmeal diuresis inAedes aegypti (L.). J. Comp. Physiol 153, 257–265. 10.1007/BF00689629.

Wu Y, Schellinger JN, Huang C-L, Rodan AR, 2014. Hypotonicity stimulates potassium flux through the WNK-SPAK/OSR1 kinase cascade and the Ncc69 sodium-potassium-2-chloride cotransporter in the *Drosophila* renal tubule. J. Biol. Chem 289, 26131–26142. 10.1074/jbc.M114.577767. [PubMed: 25086033]

Yang X, Wang Q, Cao E, 2020. Structure of the human cation–chloride cotransporter NKCC1 determined by single-particle electron cryo-microscopy. Nat. Commun 11, 1016. 10.1038/s41467-020-14790-3. [PubMed: 32081947]

Zhang S, Zhou J, Zhang Y, Liu T, Friedel P, Zhuo W, Somasekharan S, Roy K, Zhang L, Liu Y, Meng X, Deng H, Zeng W, Li G, Forbush B, Yang M, 2021. The structural basis of function and regulation of neuronal cotransporters NKCC1 and KCC2. Commun. Biol 4, 226. 10.1038/s42003-021-01750-w. [PubMed: 33597714]

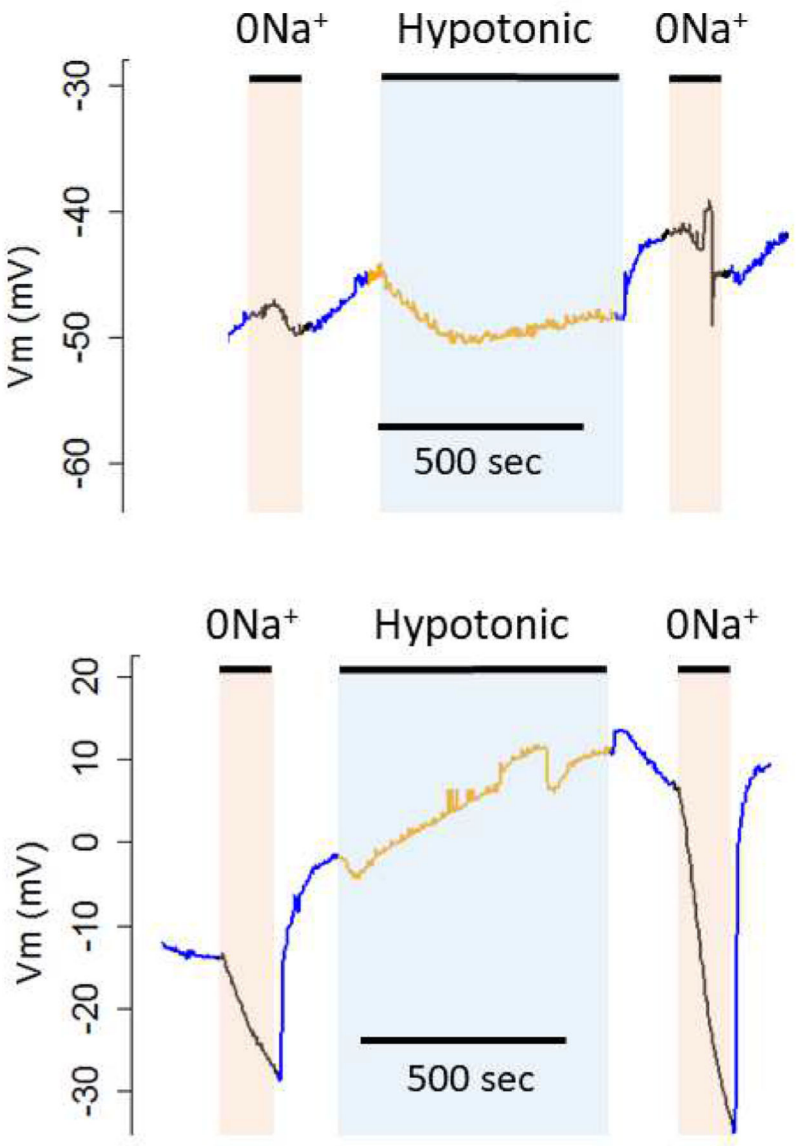

Fig. 1.

Changes in membrane potential (V_m) in response to isotonic replacement of Na^+ with NMDG before and after swelling in 50% hypotonic solution. Top: Water-injected control oocyte. Bottom: Oocyte injected with aeCCC2 cRNA.

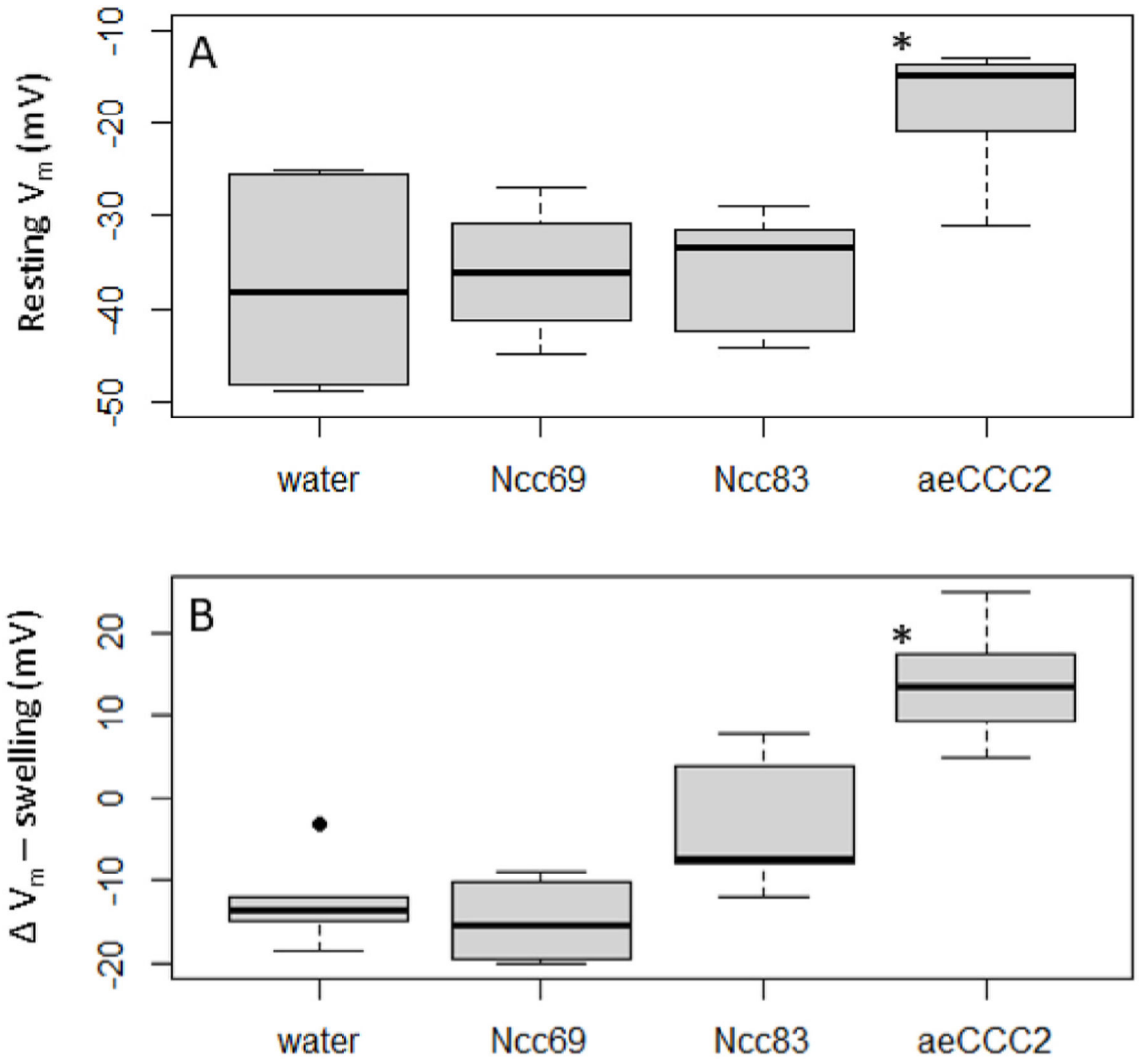

Fig. 2.

Membrane potential (V_m) responses in oocyte injected with cRNA encoding Ncc69, Ncc83, or aeCCC2 and water-injected controls. Stars indicate values significantly different than control ($p < 0.05$). A) Resting V_m in control ND96 saline. Kruskal-Wallis (chi-squared = 11.71, p-value < 0.01). B) Change in V_m during 10 min of swelling in 50% hypotonic solution. ANOVA ($F = 26.1$, $p < 0.001$).

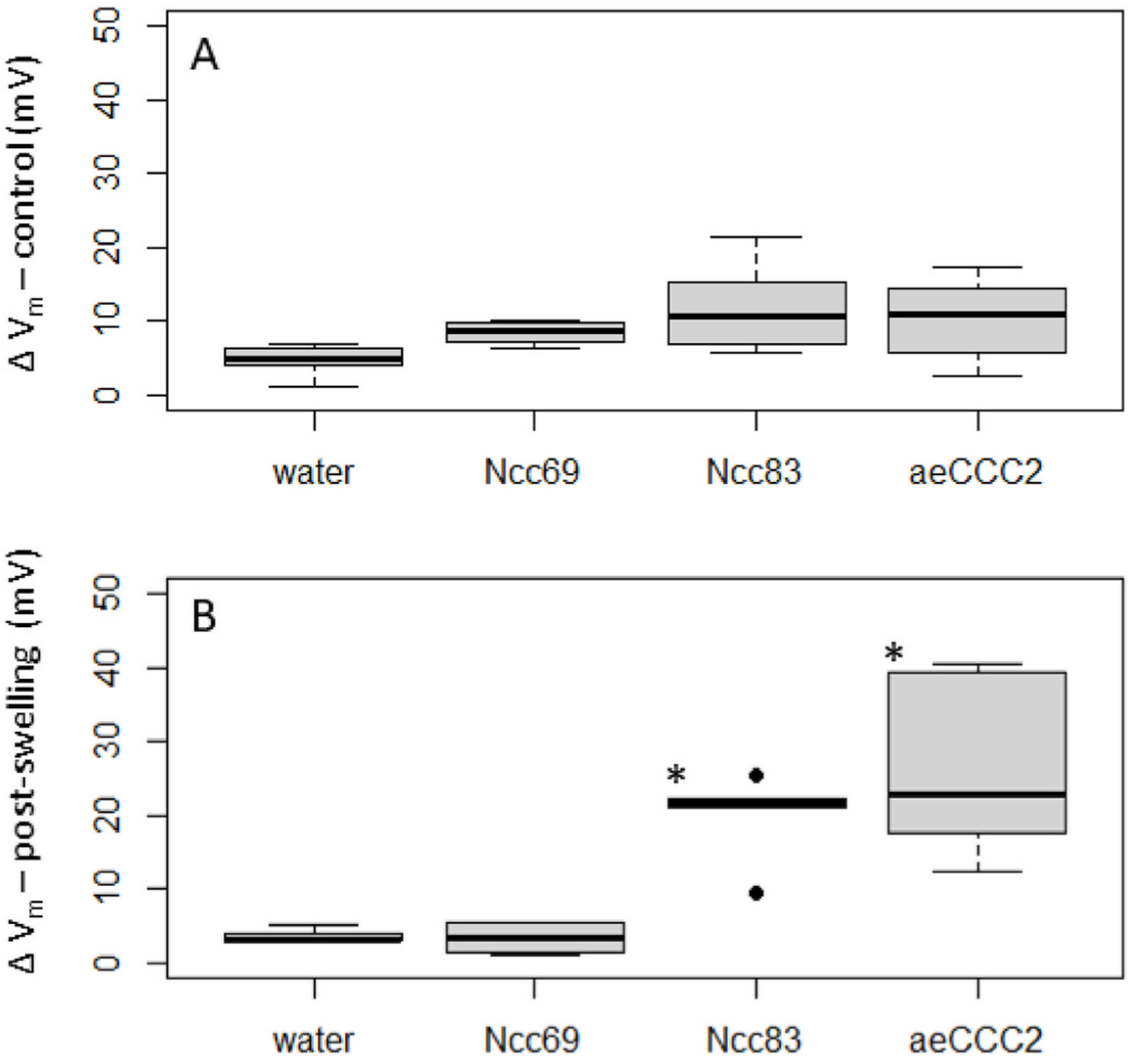

Fig. 3.

Membrane potential (V_m) changes in response to replacement of Na^+ with choline in oocyte injected with cRNA encoding Ncc69, Ncc83, or aeCCC2 and water-injected controls. Stars indicate values significantly different than control ($p < 0.05$). A) Change in V_m with Na^+ replacement prior to swelling. ANOVA ($F = 2.8$, p-value = 0.07). B) Change in V_m with Na^+ replacement following 10 min of swelling in 50% hypotonic solution. ANOVA ($F = 14.4$, $p < 0.001$).

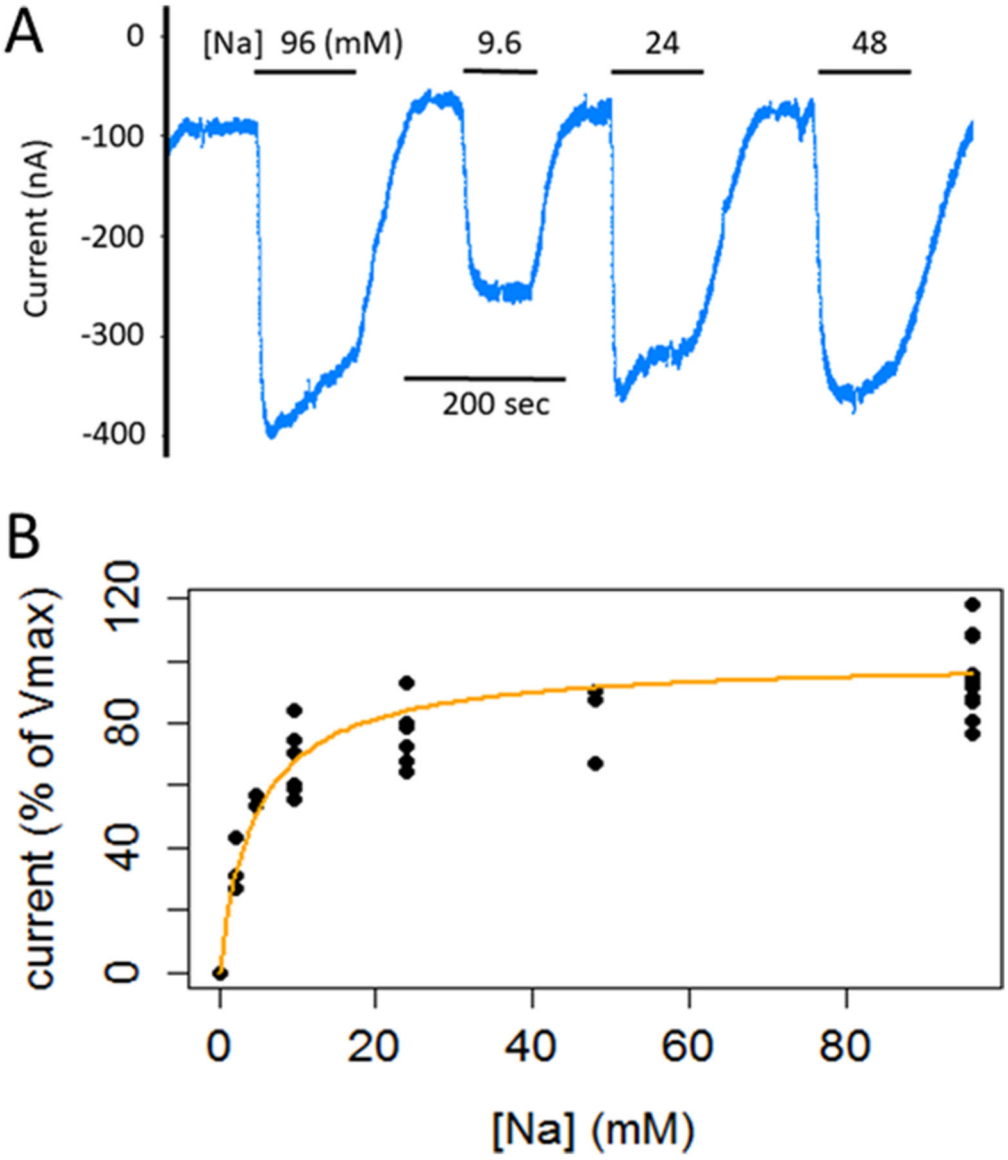

Fig. 4.

Dependence of Na^+-dependent currents on [Na^+] in voltage clamped oocytes expressing aeCCC2. A) Current tracing showing changes in current following switching from Na^+-free (isotonic substitution with choline) solutions to solutions with 9.6, 24, 48, and 96 mM Na^+. B) Summary of five experiments with currents normalized to maximum Na^+-dependent currents in 96 mM Na^+. Apparent affinity for Na^+ is 4.6 ± 1.1 mM (n = 5).

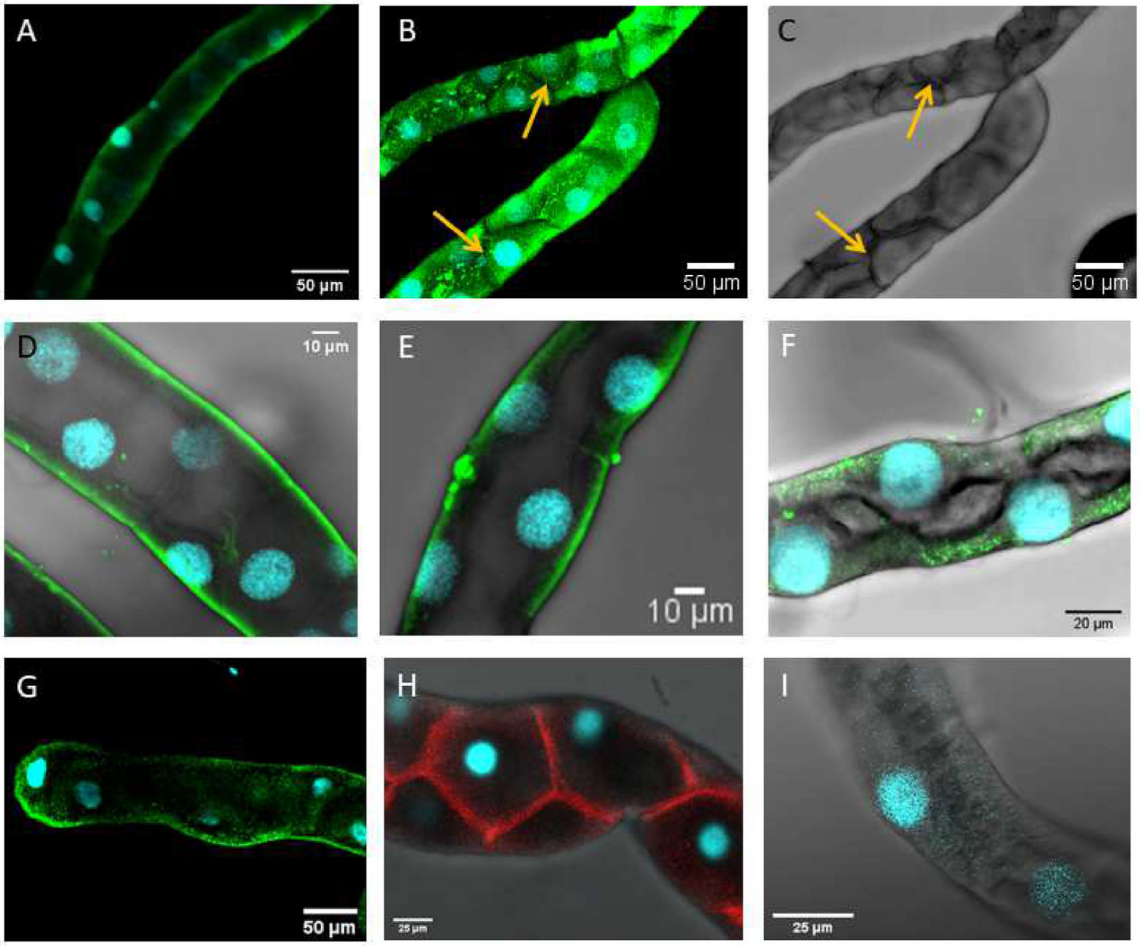

Fig. 5.

Immunohistochemical visualization of aeCCC2 in Malpighian tubules of *Aedes aegypti*. A) Larval Malpighian tubule stained with an antibody against aeCCC2 (C2–1). Average intensity projection of 37 z-slices (1 μM each). B) Larval Malpighian tubule stained with C2–1. Average intensity projection of 21 z-slices (3 μM each). Arrow points to stellate cell. C) Bright-field image corresponding to panel B. D) Proximal portion of a Malpighian tubule of larvae stained with C2–1. Average intensity projection of 43 z-slices (1 μM each). E) Distal portion of Malpighian tubule of larvae stained with C2–1. Average intensity projection of 28 z-slices (1 μM each) through the middle of the tubule. F) Distal portion of Malpighian tubule of larvae stained with C2–1. Average intensity projection of 32 z-slices (0.5 μM each) through the middle of the tubule. G) Distal Malpighian tubule of adult female stained with C2–1. Average intensity projection of 11 z-slices (13.4 μM total). H) Larval Malpighian tubules stained with an antibody against the Na^+-K^+-ATPase (A5). Average intensity projection of 8 z-slices (18.1 μM total). I) Larval Malpighian tubule with no primary antibody. Average intensity projection of 13 z-slices (10.3 μM total).

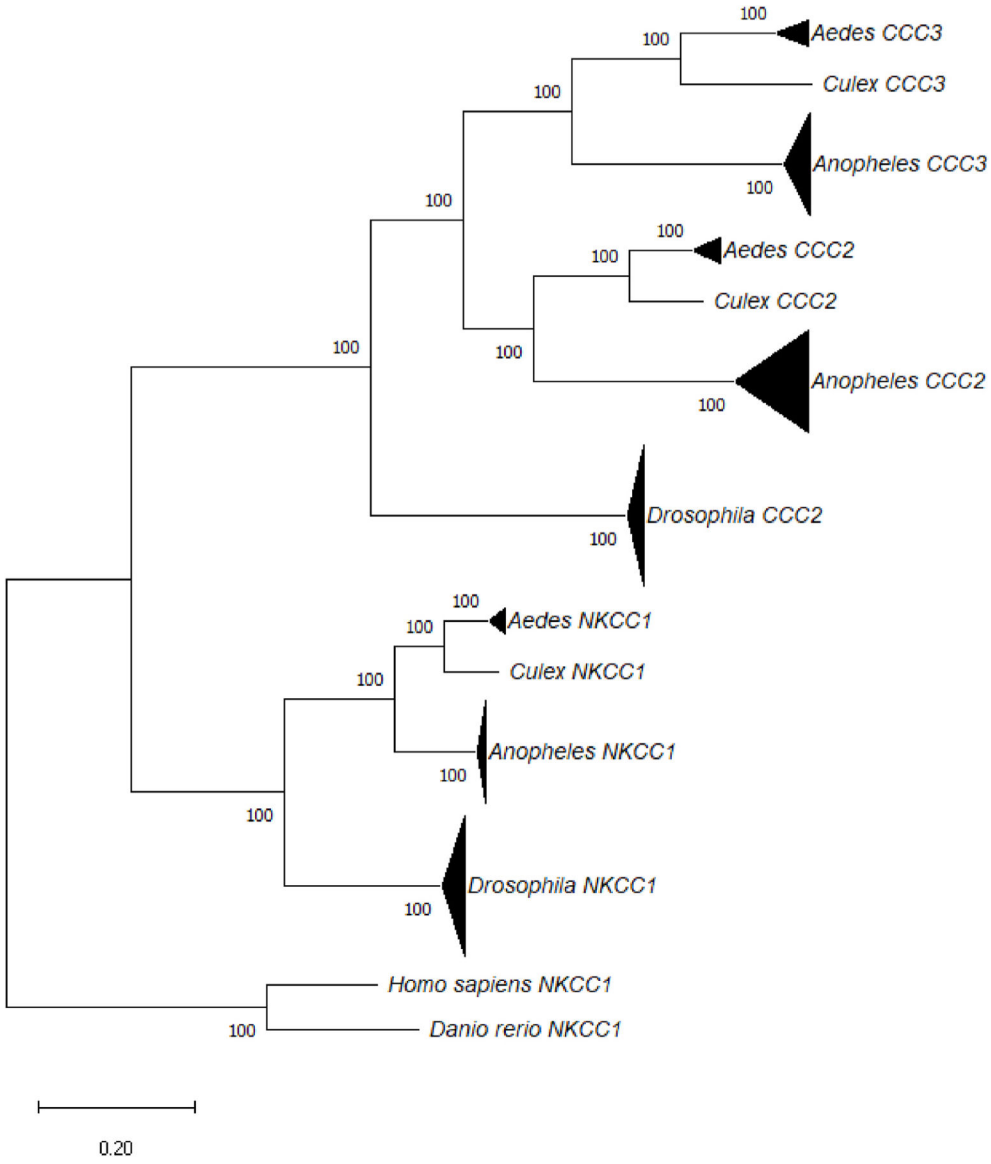

Fig. 6.

Maximum likelihood tree of sequences used in sequence analysis (Kumar et al., 2018). Bootstrap values are inferred from 100 replicates. Triangles represent clades with multiple sequences. Triangle height reflects number of sequences: 10 for *Drosophila*, 7 for *Anopheles*, and 3 for *Aedes*. Triangle width reflects divergence in substitutions per site.

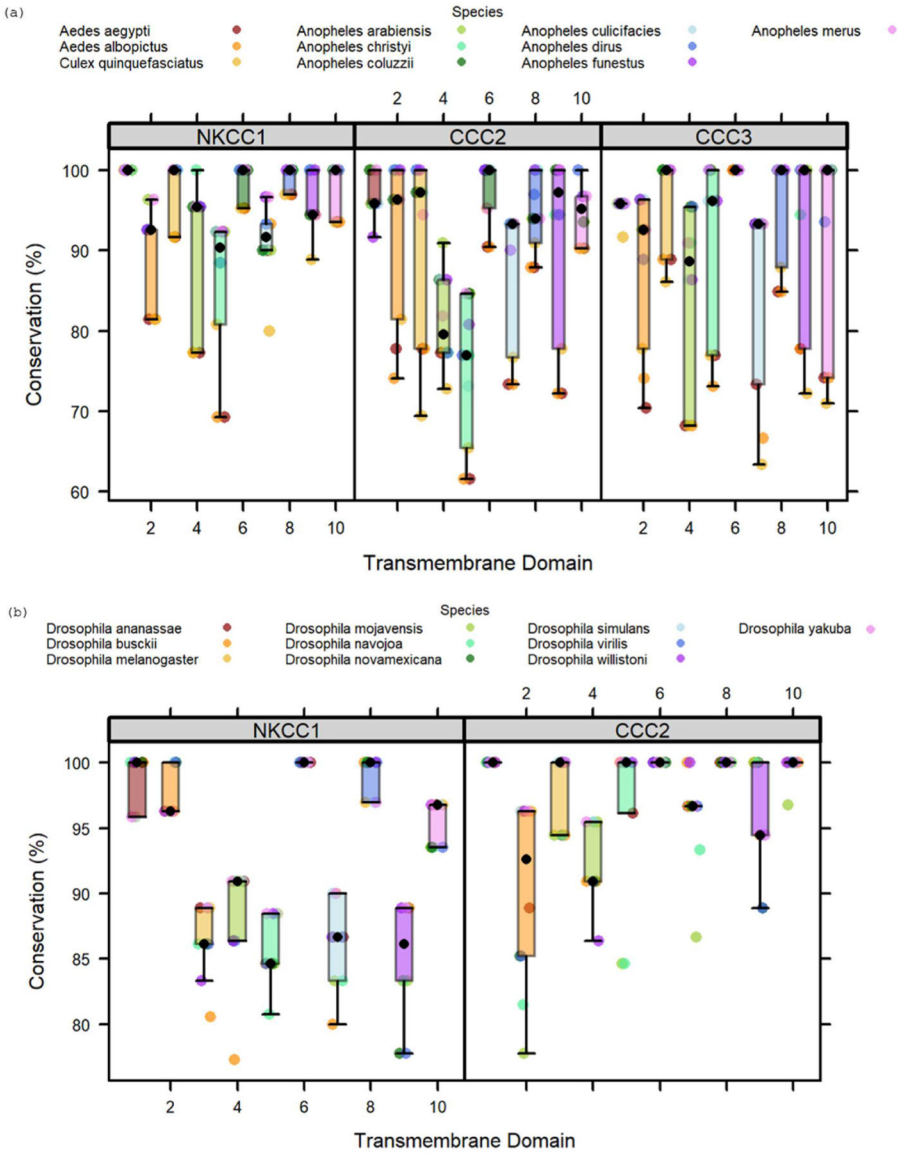

Fig. 7.

Conservation of transmembrane domains in mosquito and Drosophila NKCC1s and NaCCC2s. Conservation is reported as percent identity to paralog-specific consensus sequences. Colors of dots indicate species. A) Conservation of TMDs in the mosquito paralogs of NKCC1, CCC2, and CCC3 (n = 10 species per paralog). B) Conservation of TMDs in *Drosophila* paralogs of NKCC1, and CCC2 (n = 10 species per paralog)

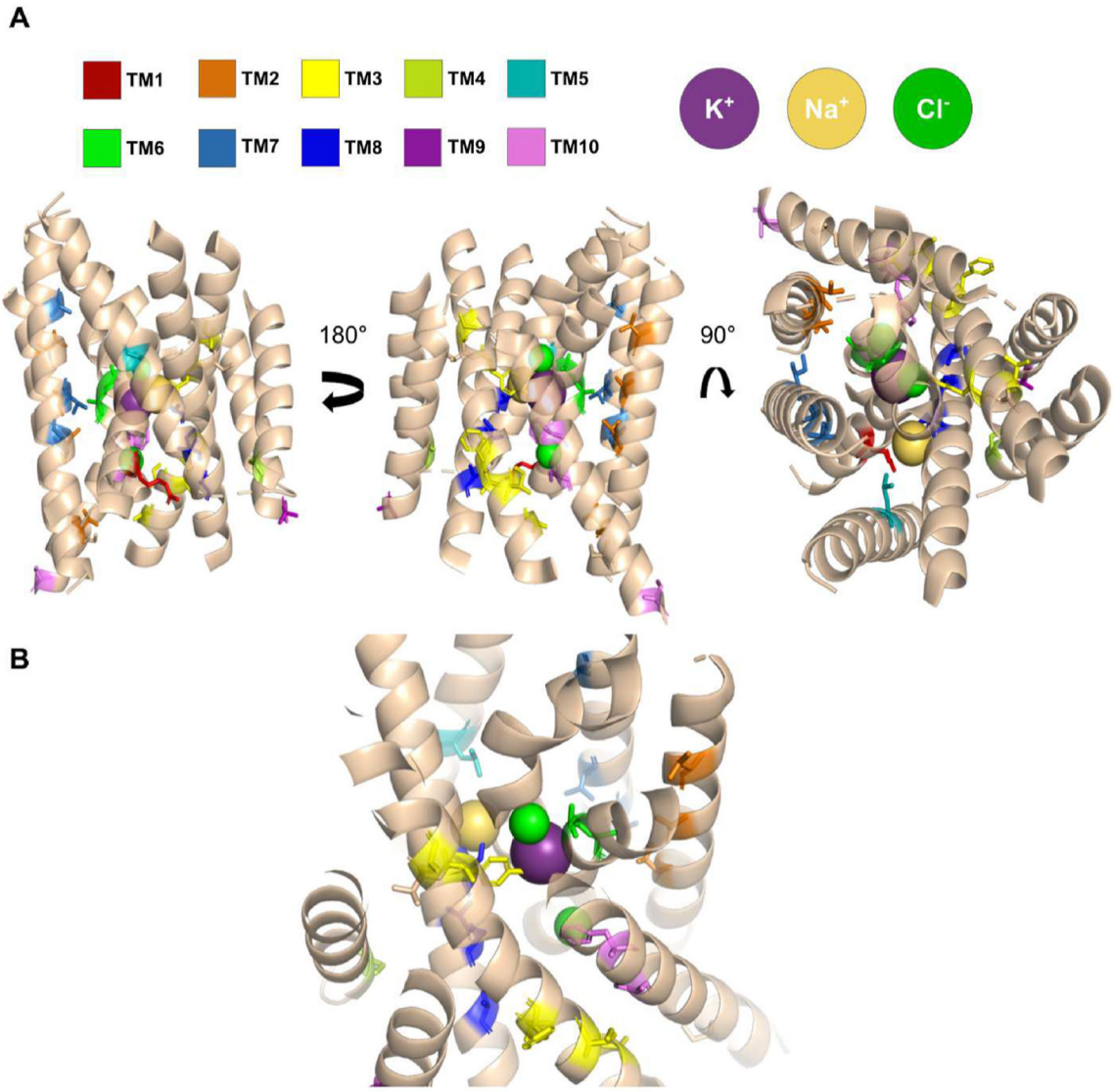

Fig. 8.

Residues conserved within paralogs but different between dipteran NKCC1 and NaCCC2s are depicted in color on a hNKCC1 monomer (PDB: 6PZT) (Yang et al., 2020). A) Side and extracellular view of hNKCC1 (TM 1–10) with annotated residues depicted in stick representation and color-coded based on TMD as shown in panel. B) A view highlighting the K^+ (purple) binding site with both Cl^- (green) and Na^+ (yellow) ions visible in frame.

Table 1

Transmembrane domain residues that are fully conserved within *Drosophila* and mosquito NKCC and NaCCC2 paralogs but different between paralogs.

TMD	aeCCC2	Ncc83	aeNKCC1	Ncc69	hsNKCC1
1	P152	P145	R185	R221	R294*
2	I181	I174	L214	L250	V323*
2	S185	S178	T218	T254	A327*
2	C189	C182	T222	T258	T331
2	L196	L189	M229	M265	T338*
3	V226	V219	I259	I295	I368*
3	V229	V222	I262	I298	I371*
3	A231	A224	S264	S300	A373
3	F232	F225	L265	L301	F374
3	N241	N234	Y274	Y310	Y383*
3	T242	T235	V275	V311	V384*
3	I243	I236	V276	V312	V385
4	C283	C276	V316	V352	S424
5	I301	I294	L334	L370	L442
6	S362	S356	A395	A432	A497*
6	V363	V357	A396	A433	A498
7	L391	L385	I423	I460	I526
7	S394	S388	T426	T463	T529
7	F401	F395	M434	M471	V536
8	T465	T463	S500	S537	S614*
8	T468	T466	A503	A540	A617
8	N469	N467	S504	S541	S618*
8	V473	V471	A508	A545	A622
8	G481	G479	C516	C553	C630
9	Y503	Y501	V538	V575	L652
10	Y533	Y531	F568	F605	F682*
10	S536	S534	A571	A608	S685
10	C543	C541	S578	S615	S692
10	A548	A546	S583	S620	S697
10	V550	V548	A585	A622	A699
11	I577	I575	V612	V649	V726
12	I593	I591	V628	V665	V742
12	F594	F592	L629	L666	L743

(*)denotes residues previously identified to have functional or structural significance.